Journal of Materials Chemistry B

ROYAL SOCIETY OF CHEMISTRY

PAPER

View Article Online
View Journal | View Issue

Cite this: J. Mater. Chem. B, 2023, 11, 5483

Amphiphilic phosphorous dendron micelles co-deliver microRNA inhibitor and doxorubicin for augmented triple negative breast cancer therapy†

Liang Chen,[abc] Mengsi Zhan,[a] Jin Li,[a] Liu Cao,[a] Huxiao Sun,[a] Régis Laurent,[bc] Serge Mignani,[de] Anne-Marie Caminade,*[bc] Jean-Pierre Majoral*[bc] and Xiangyang Shi*[ae]

Received 4th October 2022,
Accepted 22nd November 2022

DOI: 10.1039/d2tb02114e

rsc.li/materials-b

Combined chemo/gene therapy of cancer through different action mechanisms has been emerging to enhance the therapeutic efficacy towards cancer, and still remains a challenging task due to the lack of highly effective and biocompatible nanocarriers. In this work, we report a new nanosystem based on amphiphilic phosphorus dendron (1-C12G1) micelles to co-deliver microRNA-21 inhibitor (miR-21i) and doxorubicin (DOX) for combination therapy of triple negative breast cancer. The amphiphilic phosphorus dendron bearing a long linear alkyl chain and ten protonated pyrrolidine surface groups was prepared and was demonstrated to form micelles in water solution and have a hydrodynamic size of 103.2 nm. The micelles are shown to be stable, enable encapsulation of an anticancer drug DOX with optimal loading content (80%) and encapsulation efficiency (98%), and can compress miR-21i to form polyplexes to render it with good stability against degradation. The co-delivery system of 1-C12G1@DOX/miR-21i polyplexes has a pH-dependent DOX release profile, and can be readily phagocytosed by cancer cells to inhibit them due to the different anticancer mechanisms, which was further validated after intravenous injection to treat an orthotopic triple-negative breast tumor model *in vivo*. With the proven biocompatibility under the studied doses, the developed amphiphilic phosphorus dendron micelles could be developed as an effective nanomedicine formulation for synergistic cancer therapy.

10th Anniversary Statement

On the occasion to celebrate the 10th anniversary of Journal of Materials Chemistry B (JMCB), I have witnessed the continuous growth the journal, a leading Royal Society of Chemistry (RSC) journal publishing papers in the fields of all aspects of biomaterials research. Until now, our group has published 31 papers in JMCB in the area of drug/gene delivery, molecular imaging, biosensing, and tumor therapy/theranostics. I have also been an active reviewer for JMCB, and was awarded as an excellent reviewer for JMCB in 2020 by the RSC. During my experience with JMCB, my team members and collaborators, as well as my colleagues working in the field of biomaterials all feel that JMCB is an excellent journal and forum to publish biomaterials-related research work in terms of its processes of peer review, editorial work, production, and distribution.

[a] *State Key Laboratory for Modification of Chemical Fibers and Polymer Materials, Shanghai Engineering Research Center of Nano-biomaterials and Regenerative Medicine, College of Biological Science and Medical Engineering, Donghua University, Shanghai, 201620, People's Republic of China. E-mail: xshi@dhu.edu.cn*

[b] *Laboratoire de Chimie de Coordination du CNRS, 205 Route de Narbonne, BP 44099, 31077, Toulouse CEDEX 4, France. E-mail: anne-marie.caminade@lcc-toulouse.fr, jean-pierre.majoral@lcc-toulouse.fr*

[c] *Université de Toulouse, UPS, INPT, 31077, Toulouse CEDEX 4, France*

[d] *Université Paris Descartes, PRES Sorbonne Paris Cité, CNRS UMR 860, Laboratoire de Chimie et de Biochimie Pharmacologiques et Toxicologique, 45, rue des Saints Péres, 75006, Paris, France*

[e] *CQM – Centro de Química da Madeira, Universidade da Madeira, Campus da Penteada, 9020-105, Funchal, Portugal*

† Electronic supplementary information (ESI) available: Additional experimental details and data. See DOI: https://doi.org/10.1039/d2tb02114e

Introduction

Although considerable progresses have been made in the early diagnosis and treatment, multidrug resistance and side-effect of traditional chemotherapeutics are still major bottle-neck problems to be solved for effective cancer therapy. Therefore, various strategies have been developed to overcome these problems. Among them, the combined drug/gene co-delivery strategy has been paid much attention to enhance the efficacy of cancer therapy through the induced synergy exerted by each drug with its inherent mechanistic action.[1–3]

MicroRNAs (miRNAs) are known to be a family of small, endogenous noncoding RNAs that can post-transcriptionally

regulate the translation and stability of mRNAs.[4,5] The disorder of miRNAs has been disclosed in a variety of cancer types and is considered as a sign of cancer.[6] Importantly, due to the complexity of cancer-associated signal networks, the multiple targeting capability of tumor suppression miRNAs has attracted extensive attention in improving the cancer therapy efficacy.[6] In this context, anti-cancer therapies based on miRNA have been developed either alone or together with chemical drugs, aiming to improve the therapeutic efficacy.[7] In particular, microRNA-21 (miR-21) has been noticed to be highly expressed in triple negative breast cancer (TNBC), pancreatic cancer, or other types of cancer.[8,9] The high expression of miR-21 is found to promote tumor growth and proliferation by acting on the phosphatase and tensin homolog (PTEN)-associated pathways.[8–10]

A recent study showed that knocking down of miR-21 has marginal impact on the cancer cell viability, but the inhibition of cell growth was improved when the cancer cells were treated with an additional anticancer drug. This suggests that the chemotherapy effect of cancer cells can be sensitized through inhibition of miR-21.[10] Previously, we have shown that generation 5 poly(amidoamine) (PAMAM) dendrimer-entrapped gold nanoparticles (NPs) can be utilized as a carrier to co-deliver anticancer drug gemcitabine and miR-21i to pancreatic cancer cells, thus significantly enhancing the therapeutic efficacy of cancer cells in comparison to the single delivery of gemcitabine.[11] In another study, hyaluronic acid-chitosan NPs were used to encapsulate microRNA and doxorubicin (DOX) for improved therapy of cancer cells.[3] These co-delivery systems are able to encapsulate and controllably deliver different payloads of therapeutics to the site of disease to exert their therapeutic functions in a synergistic fashion.[10–15] For the developed nanomedicine platforms, it is of great importance to effectively load both drug and genetic material with a good morphology control.[3,16–21] An ideal carrier system should have a positive surface potential allowing for effective compression of the negatively charged genetic materials, and hydrophobic interior cavities allowing for effective encapsulation of hydrophobic anticancer drugs. Although PAMAM dendrimers[8] or newly developed core–shell tecto dendrimers[11] were demonstrated to have such features, the volume of their internal cavities is quite limited.

In view of the recent developments, amphiphilic dendrimers or dendrons that can form micelles or dendrimersomes have received a great deal of attention for co-delivery of drugs and genes.[16,22,23] The reported dendritic polymers based on PAMAMs have a quite flexible molecular structure, which is not ideal for enhanced gene delivery. In a very recent study,[24] we have shown that core–shell tecto dendrimers possessing rigid core of phosphorous dendrimers and PAMAM shell dendrimers display much more enhanced gene compression and delivery efficiency than the counterpart having both PAMAM core and shell dendrimers. Very recently, we have shown that amphiphilic phosphorous dendrons with either negatively charged tyramine-bearing two dimethylphosphonate sodium salt[25] or positively charged protonated pyrrolidine moieties[26] can be used to encapsulate hydrophobic drugs to fight inflammatory disease or cancer. Therefore, it is quite logic to develop a phosphorous dendron-based micellar system to co-deliver both chemical drug and gene (*e.g.*, miR-21i) for enhanced cancer therapy.

Here, in this present study, we introduced a novel amphiphilic phosphorous dendron material to form micelles. The amphiphilic phosphorus dendron (1-C12G1, Scheme 1A and Fig. 1) bearing a long linear alkyl chain ($C_{12}H_{25}$) and ten protonated pyrrolidine groups on the surface was first synthesized and then assembled to form stable nanomicelles for encapsulation of anticancer drug DOX and complexation of miR-21i. The physicochemical property of the dendrons and dendron micelles, drug release profile, anticancer cytotoxicity, and cellular uptake behavior were systematically investigated, and the co-delivery of DOX and miR-21i for effective cancer therapy was validated using an orthotopic triple-negative breast tumor model (Scheme 1B). According to our literature investigation, this study represents a very first example associated to the use of phosphorous dendron micelles for drug/gene co-delivery to fight cancer.

Results and discussion

Preparation and characterization of amphiphilic phosphorus dendrons

As illustrated in Fig. 1, a new amphiphilic phosphorus dendron with hydrophobic alkyl chain ($C_{12}H_{25}$), rigid structure (benzene ring and double bond) and hydrophilic group (protonated pyrrolidine) was synthesized. This dendron was thoroughly characterized with various NMR techniques (Fig. S1–S4, ESI†). Meanwhile, the 1-C12G1 dendrons were dissolved in water and the ability to form micelles was examined through the critical micelle concentration (CMC) determination (Fig. 2A). Clearly, the CMC of the micelles was determined to be 151 μM. Dynamic light scattering was also employed to determine the hydrodynamic diameter and polydispersity index (PDI) of the micelles. The 1-C12G1 dendron micelles display a hydrodynamic diameter about 103.2 nm (Fig. S5A, ESI†) with a narrow distribution (PDI = 0.798, Table S1, ESI†). After dilution to a concentration around 5 times lower than the CMC, the hydrodynamic diameter of the micelles does not seem to have any significant change (99 nm, Fig. S5B, ESI†) and the PDI was even lower (0.314, Table S1, ESI†). This suggests that the dendron micelles generated by 1-C12G1 display a good colloidal stability. The morphology of the 1-C12G1 micelles was also examined by transmission electron microscopy (TEM), and the 1-C12G1 micelles exhibit a spherical shape with an mean size of 25 nm (Fig. S5C, ESI†).

Preparation and characterization of 1-C12G1@DOX and 1-C12G1@DOX/miR-21i polyplexes

We next loaded the anticancer drug DOX within the micelles to form the 1-C12G1@DOX complexes. The loading content and encapsulation efficiency of the micelles were first investigated by changing the 1-C12G1/DOX molar ratios. As shown in

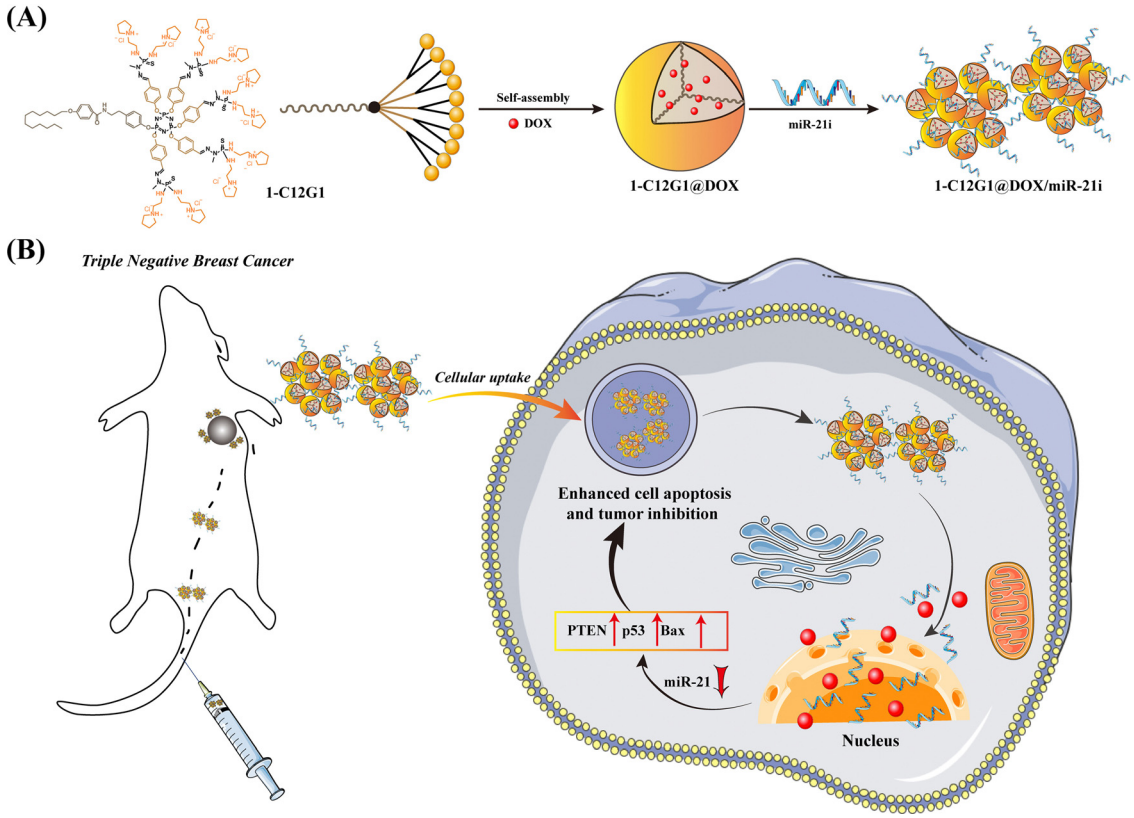

Scheme 1 Preparation of 1-C12G1@DOX/miR-21i Polyplexes (A). Co-delivery Treatment of a Tumor Model *in vivo* (B).

Table 1, at the 1-C12G1@DOX molar ratio of 1 : 25, both the loading content and encapsulation efficiency are quite high, reaching 79.2% and 97.9%, respectively. Thus, the 1-C12G1@DOX with the molar ratio of 1 : 25 was chosen for following investigations. The high drug-loading capacity may be caused by the molecular structure of 1-C12G1 with rigid hydrophobic branches, generating micelles with large hydrophobic cores for encapsulation of significant amount of drug, similar to the micelles formed from lipids.[27]

To further investigate the colloidal stability of 1-C12G1@DOX micelles, the hydrodynamic diameter of 1-C12G1@DOX was checked at different concentrations (Fig. S6, ESI†). At a high DOX concentration, the hydrodynamic diameter of the 1-C12G1@DOX micelles is around 221 nm (PDI = 0.286, Fig. S6A and Table S1, ESI†). After 10 times dilution, the hydrodynamic diameter and PDI of the micelles do not show any appreciable changes (218 nm and 0.290, Fig. S6B and Table S1, ESI†). This means that the drug-loaded micelles also possess good colloidal stability, similar to the drug-free micelles. The morphology of the 1-C12G1@DOX micelles was also observed by TEM (Fig. S6C, ESI†), and the drug-loaded micelles are spherical, similar to the drug-free ones. The larger mean size of the 1-C12G1@DOX micelles (42 nm) than that of the drug-free ones should be due to the DOX loading that expands the overall geometry of the micelles. Note that the hydrodynamic sizes of the 1-C12G1 and 1-C12G1@DOX micelles are much larger than those of the corresponding micelles measured by TEM. This should be because TEM measures the size of single 1-C12G1 and 1-C12G1@DOX micelles in a dry state, while dynamic light scattering measures the hydrodynamic sizes of the 1-C12G1 and 1-C12G1@DOX micelles in aqueous solution, which usually reflects the micelles with certain degree of aggregation.[26] The fluorescence properties of free DOX and 1-C12G1@DOX were investigated (Fig. 2B and C). Due to fluorescence quenching effect similar to our previous work,[26] the free DOX exhibits higher fluorescence intensity than 1-C12G1@DOX at the same DOX concentration. Meanwhile, both free DOX and 1-C12G1@DOX display stronger fluorescence intensity at a low concentration than at a high concentration.

Next, we used 1-C12G1@DOX micelles to compact miR-21i to form 1-C12G1@DOX/miR-21i polyplexes. Gel retardation assay data shown in Fig. S7A (ESI†) reveal that the miR-21i can be fully compacted by the 1-C12G1@DOX micelles at an N/P ratio of 1 : 1 or above. Then, we examined the stability of 1-C12G1@DOX/miR-21i polyplexes (N/P value = 5 : 1) exposed to normal saline (NS) at 37 °C (Fig. S7B, ESI†). Clearly, the miR-21i complexed with 1-C12G1@DOX micelles can be protected from degradation for up to 12 h and 24 h. In contrast, naked miR-21i is not stable and can be degraded to have diminished bands under the same conditions.

The hydrodynamic size and surface potential of the polyplexes were key factors to assess the performance of gene cargos.[28] We then examined the zeta potential and mean

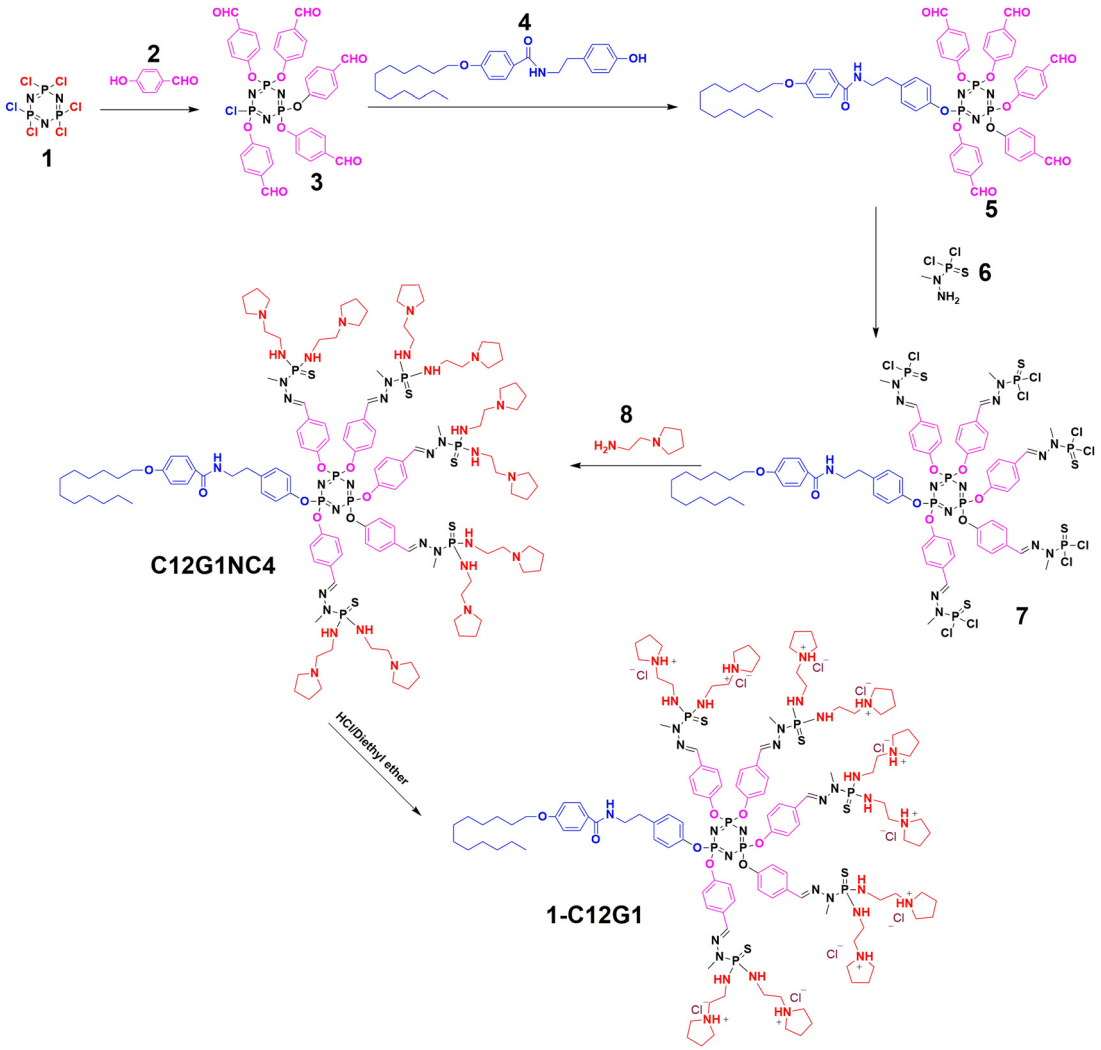

Fig. 1 Synthesis of amphiphilic phosphorus dendrons.

hydrodynamic diameter of the polyplexes. As shown in Fig. 2D and E, with the increase of N/P ratio, the compaction interaction between 1-C12G1@DOX and miR-21i can be saturated to lead to insignificant changes of the surface potential of the polyplexes as the surface of the polyplexes is fully covered with the positively charged dendrons. Meanwhile, more dendrons contribute to the compression of miR-21i to cause the size decrease of the polyplexes until reaching the point of saturation. According to the literature,[29] vector/gene polyplexes with a positive surface potential and a size of around 200 nm are suitable for gene delivery purpose. Therefore, we selected an N/P ratio of 5 : 1 to prepare the polyplexes for later experimental investigations.

To evaluate the stability of the 1-C12G1@DOX/miR-21i polyplexes, their hydrodynamic size in both NS and complete cell culture medium at 37 °C was examined for different time periods (Fig. 2F). No obvious aggregation of polyplexes were observed and the polyplexes show approximately similar sizes ranging from 225 to 270 nm for 4 days. This indicates that the 1-C12G1@DOX/miR-21i polyplexes display desired stability, which is ready for further studies. Meanwhile, the 1-C12G1@DOX/miR-21i polyplexes have similar hydrodynamic diameter and PDI at different concentrations (Fig. S8 and Table S1, ESI†), reflecting their good colloidal stability. Interestingly, the 1-C12G1@DOX/miR-21i polyplexes exhibit a smaller mean size (36 nm, Fig. S8C, ESI†) than the 1-C12G1@DOX (42 nm) before miR-21i complexation, which may be caused by the compaction of the micelles after electrostatic interaction with the miR-21i.

For an ideal drug delivery system employed in cancer therapy, it is crucial to have the therapeutic agent to be controllably released at the tumor site, thus avoiding the non-desired toxicity to normal tissues. Since the tumor lesion is generally slightly acidic in pH, acid-triggered fast drug release at tumor site is undoubtedly beneficial to improve the cancer therapy performance.[30,31] Next, the release profile of DOX from the 1-C12G1@DOX/miR-21i was investigated at 37 °C and in phosphate buffer at both pH 5.5 and pH 7.4 (Fig. S9, ESI†). DOX release from the polyplexes can reach around 51% and 30% within the first 10 h at pH 5.5 and pH 7.4, respectively, after which continuous slow release of DOX remains. At the same

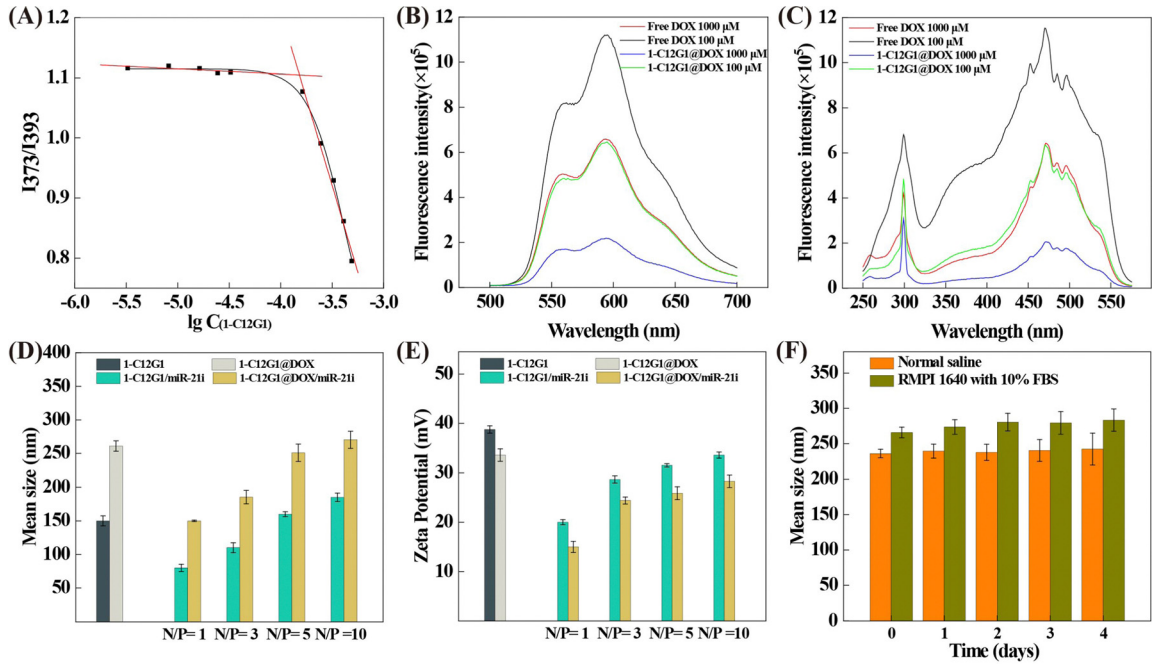

Fig. 2 Determination of the CMC of 1-C12G1 micelles using the fluorescent dye pyrene (A). Fluorescence emission (B) and excitation (C) spectra of free DOX and 1-C12G1@DOX (excitation wavelength: 365 nm, and emission wavelength: 595 nm). Mean hydrodynamic diameter (D) and zeta potential (E) of 1-C12G1, 1-C12G1@DOX, 1-C12G1/miR-21i and 1-C12G1@DOX/miR-21i. (F) Stability assessments of 1-C12G1@DOX/miR-21i in different aqueous media as assessed by their mean hydrodynamic size changes at 37 °C for different time periods.

Table 1 Optimizing the loading content and encapsulation efficiency of 1-C12G1 micelles

1-C12G1 : DOX mass ratio	Drug encapsulating efficiency (wt%)	Drug loading content (wt%)
1 : 15	99.81 ± 0.5	69.9 ± 0.4
1 : 20	98.11 ± 0.7	75.4 ± 0.5
1 : 25	97.94 ± 1.1	79.2 ± 0.8
1 : 30	83.60 ± 1.3	82.1 ± 1.0
1 : 35	77.17 ± 2.8	78.3 ± 1.5

time point, the DOX release at pH 5.5 is faster than at pH 7.4, likely owing to the protonation of DOX at a lower pH to lead to increased water solubility of DOX, in agreement with the literature.[32]

Enhanced therapy of cancer cells *in vitro*

Previous studies have shown that miRNAs have synergistic antitumor effects in combination with conventional chemotherapy.[3,33,34] Hence, we evaluated the antiproliferation efficiency of the developed 1-C12G1@DOX/miR-21i polyplexes using two cell lines, including normal NIH-3T3 cells and MDA-MB-231 cells. As can be seen in Fig. 3A, the antiproliferation effect of free DOX towards normal NIH-3T3 cells is higher than that of 1-C12G1@DOX and 1-C12G1@DOX/miR-21i polyplexes at the same DOX concentrations, presumably due to the fact that the sustained DOX release from the micelles leads to a lower DOX concentration for cell treatment. Meanwhile, the viability of NIH-3T3 cells incubated with 1-C12G1 or 1-C12G1/miR-21i does not seem to have any significant changes. As shown in Fig. 3B, for cancer cells, no apparent cell death can be observed in the 1-C12G1-treated cells, implying the good cytocompatibility of drug-free 1-C12G1 dendron micelles. The MDA-MB-231 cells treated with 1-C12G1/miR-21i show a reduced cell viability with the increase of equivalent DOX concentration, suggesting that the delivery of miR-21i to cells may trigger the death of MDA-MB-231 cells. Free DOX, 1-C12G1@DOX and 1-C12G1@DOX/miR-21i all exhibit remarkable cytotoxicity to MDA-MB-231 cells in a DOX concentration-dependent fashion. Free DOX displays slightly higher cytotoxicity than the 1-C12G1@DOX micelles, but lower cytotoxicity than the 1-C12G1@DOX/miR-21i polyplexes under the identical DOX doses. This suggests that the 1-C12G1@DOX/miR-21i polyplexes can fully utilize the active gradients of both DOX and miR-21i to have a synergistic therapy effect through combination of different mechanisms. The IC_{50} values of the different formulations are shown in Fig. S10 (ESI†), and the anticancer efficiency can be ranked in an order of 1-C12G1@DOX/miR-21i (0.073 μM) > free DOX (0.37 μM) > 1-C12G1@DOX (0.85 μM). The IC_{50} of 1-C12G1@DOX/miR-21i is approximately 5 times lower than that of free DOX, demonstrating the excellent synergistic therapy effect by integration of both DOX and miR-21i within one micellar formulation.

The intracellular uptake was qualitatively monitored by confocal and fluorescence microscopies (Fig. 4). Clearly, after the cells were incubated for 4 h with free DOX, 1-C12G1@DOX and 1-C12G1@DOX/miR-21i, significant fluorescent signals of DOX (red) are shown in the cytoplasm. The overlapped blue (nucleus), red and green (β-actin) fluorescence images show

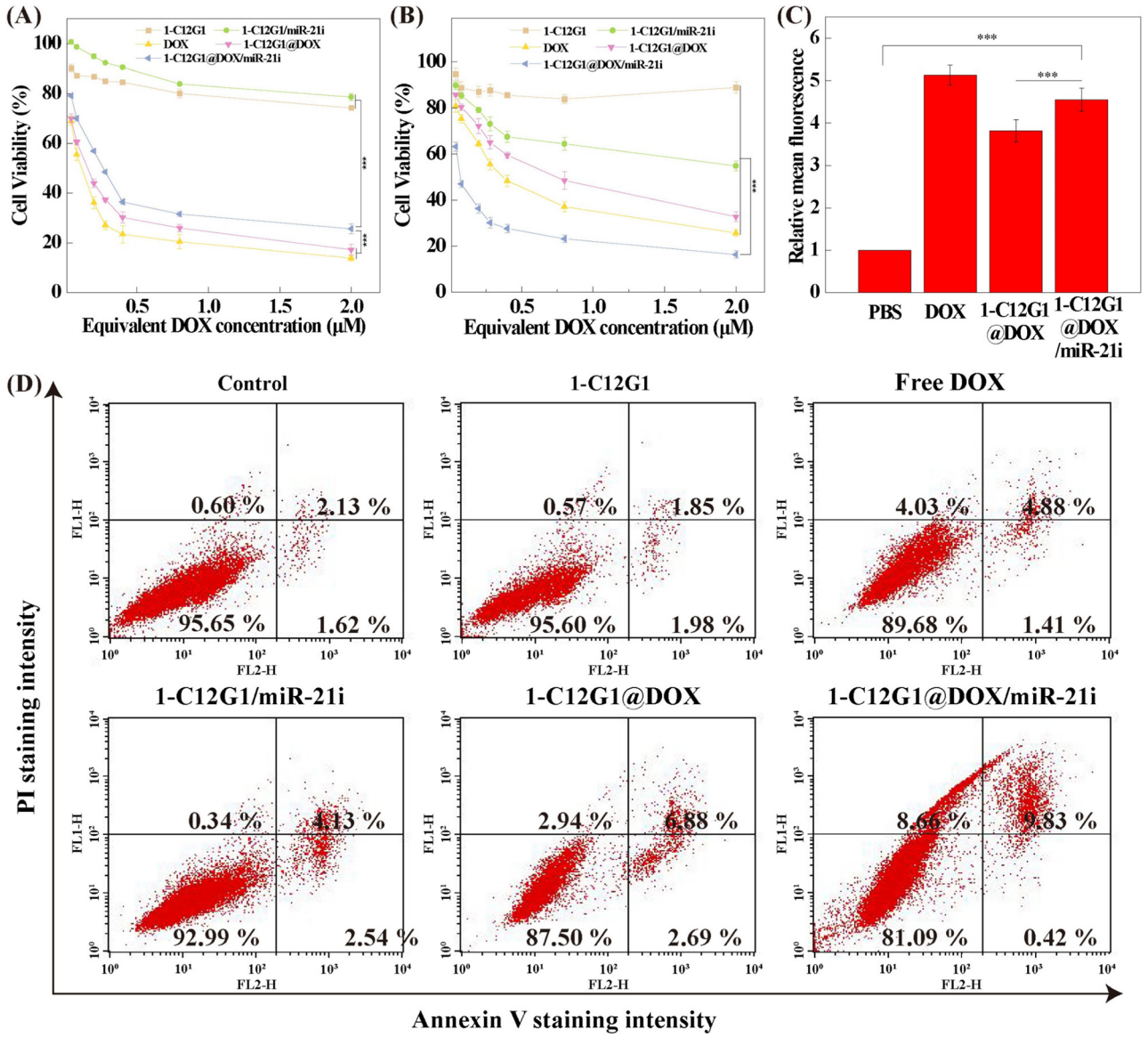

Fig. 3 Concentration-dependent cell viability of NIH-3T3 (A) and MDA-MB-231 (B) cells treated with 1-C12G1, 1-C12G1/miR-21i, 1-C12G1@DOX or 1-C12G1@DOX/miR-21i assessed by CCK-8 assay. Data were shown as mean ± SD (n = 6). (C) Relative mean fluorescence intensity of MDA-MB-231 cells incubated with free DOX, 1-C12G1@DOX or 1-C12G1@DOX/miR-21i (the equivalent concentration of DOX was 1 μM) assayed by flow cytometry. (D) Apoptosis of MDA-MB-231 cells incubated with 1-C12G1, free DOX, 1-C12G1/miR-21i, 1-C12G1@DOX or 1-C12G1@DOX/miR-21i (the equivalent DOX concentration was 1 μM) as assayed by flow cytometry. Phosphate buffered saline (PBS) was utilized as control.

that the red fluorescence associated to DOX is partly colocalized within the cytoplasm and the cell nuclei, suggesting that either free DOX or DOX within the micelles can be internalized firstly within the cytoplasm and then go into the cell nuclei. Similar results can also be obtained through fluorescence microscopic imaging (Fig. S11, ESI†).

The cellular uptake of free DOX, 1-C12G1@DOX and 1-C12G1@DOX/miR-21i by MDA-MB-231 cells and NIH-3T3 cells were further confirmed by flow cytometry (Fig. 3C, and Fig. S12–S14, ESI†). These results imply that both MDA-MB-231 and NIH-3T3 cells can be effectively delivered with DOX by the 1-C12G1-based micelles.

To further investigate if there are synergistic effects of miR-21i and DOX in cell apoptosis, MDA-MB-231 cells were treated with free DOX, 1-C12G1@DOX or 1-C12G1@DOX/miR-21i and analyzed by flow cytometry (Fig. 3D and Fig. S15, ESI†). No obvious cell apoptosis can be seen in the group of drug-free 1-C12G1 micelles, similar to the PBS control group. Our results suggest that the 1-C12G1 micelles have a good cytocompatibility in the concentration range investigated. However, cells treated with the 1-C12G1/miR-21i have an apoptosis percentage of 7.06% ± 0.24%, which is significantly higher than the PBS control group (4.21% ± 0.29%, $p < 0.001$), implying the gene therapy efficacy of the miR-21i. Additionally, all of the other three DOX-containing groups exhibit obvious cell apoptosis effect compared to the control group. Similar to our expectation, the cell apoptosis percentage of the 1-C12G1@DOX/miR-21i group

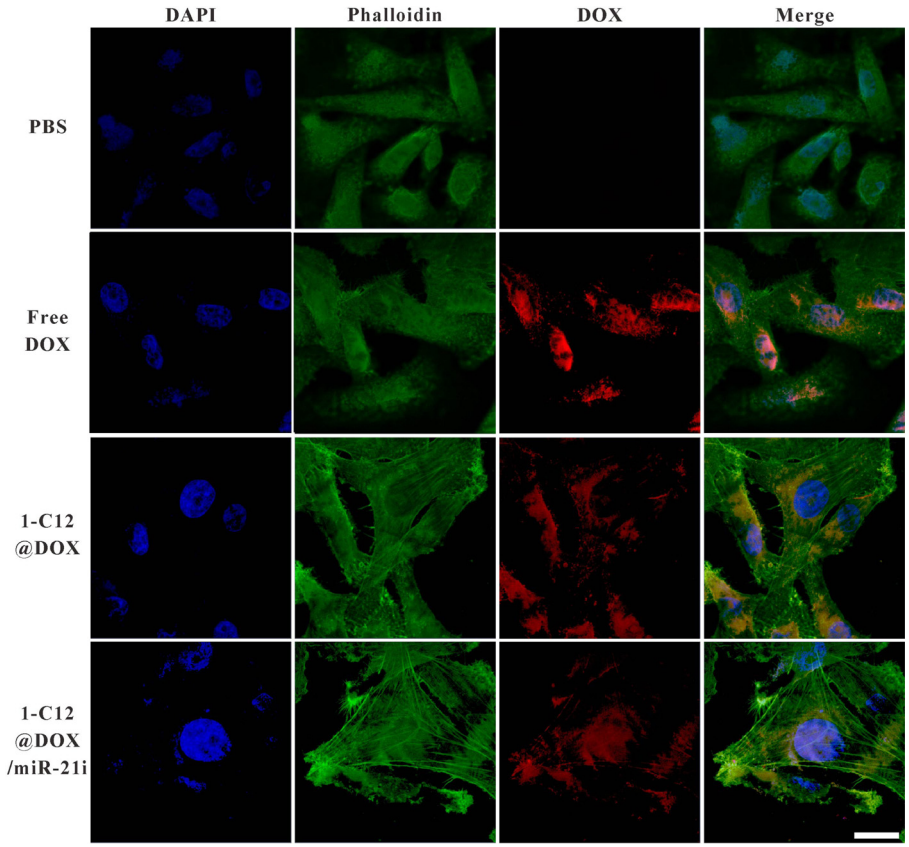

Fig. 4 Laser confocal microscopic images of MDA-MB-231 cells treated with free DOX, 1-C12G1@DOX or 1-C12G1@DOX/miR-21i for 4 h (the equivalent DOX concentration was 1 μM). Scale bar in each panel represents 200 μm.

(10.5 ± 0.2%) is higher than that of the free DOX (6.1 ± 0.2%, $p < 0.001$) and 1-C12G1@DOX (9.47% ± 0.07%, $p < 0.05$) groups. The obtained data confirmed the synergistic chemo/gene therapeutic efficacy of such a co-delivery system.

The cell apoptosis-associated proteins were examined through western blotting *in vitro* to further elucidate the molecular mechanism of the cell apoptosis (Fig. 5). Significantly increased expression of BAX, p53 and PTEN is observed in cells incubated with free DOX, 1-C12G1/miR-21i, 1-C12G1@DOX and 1-C12G1@DOX/miR-21i. Apparently, in the presence of either miR-21i or DOX, the apoptosis of MDA-MB-231 cells can be promoted. Moreover, the expression levels of all

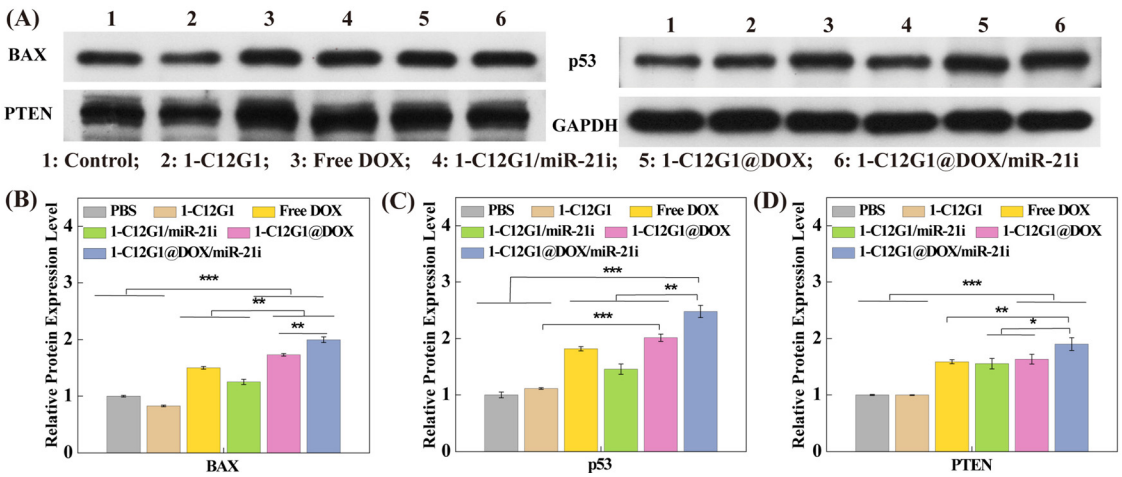

Fig. 5 (A) Western Blot assay of the expression of protein relevant to cell apoptosis in MDA-MB-231 cells treated with 1-C12G1, free DOX, 1-C12G1/miR-21i, 1-C12G1@DOX or 1-C12G1@DOX/miR-21i (the equivalent concentration of DOX was 1 μM). PBS was used as control. Quantification of BAX (B), p53 (C), and PTEN (D) proteins relevant to cell apoptosis from the western blotting data *in vitro* (* $p < 0.05$, ** $p < 0.01$, and *** $p < 0.005$, respectively).

apoptosis-related proteins are the highest in the group of 1-C12G1@DOX/miR-21i among all groups ($p < 0.05$). These results confirm the synergistic chemo/gene therapeutic efficacy of such a co-delivery system, in agreement with the apoptosis assay results obtained by flow cytometry.

Co-delivery treatment of a tumor model *in vivo*

Next, an orthotopic model of TNBC was built to assess the synergistic therapeutic efficacy of 1-C12G1@DOX/miR-21i polyplexes *in vivo* (Fig. 6A and Fig. S16, ESI†). Administration of free DOX, 1-C12G1/miR-21i, 1-C12G1@DOX or 1-C12G1@DOX/miR-21i polyplexes leads to great tumor growth inhibition. In contrast, the drug-free 1-C12G1 group does not seem to have any inhibtion effect, similar to the NS control group. During the entire treatment period, mice in the NS, 1-C12G1, 1-C12G1/miR-21i, 1-C12G1@DOX or 1-C12G1@DOX/miR-21i treatment groups behave normally, and the mouse body weight in these different groups has no significant changes (Fig. 6B). This implies that the developed 1-C12G1 micelles and the associated polyplexes have no appreciable *in vivo* toxicity during the experimental investigation period. To be opposed, mice treated with free DOX display apparent weight loss. Two mice treated with the free DOX are dead during the treatment period (Fig. 6C), while is in contrast to all other groups within 15 days. This should be due to the free DOX-induced high toxicity.[35–37]

On the 16th day, the tumor tissues were extracted to separate the tumor cells for western blot assay of apoptosis-related proteins (Fig. 6D). Remarkably, in the group of 1-C12G1@DOX/miR-21i polyplexes, the tumor cells display the highest expression levels of BAX, PTEN and p53 proteins among all groups ($p < 0.01$), which is in good consistence with the *in vitro* therapeutic results (Fig. 6E–G). These data imply that the synthesized amphiphilic phosphorus dendron micelles are able to encapsulate DOX and condense miR-21i to implement a synergistic tumor therapy effect *in vivo*.

Then, the tumor tissue samples were further examined *via* H&E (Fig. S17, ESI†) and TUNEL (Fig. 7) staining. Clearly, tumors treated with the 1-C12G1@DOX/miR-21i polyplexes reveal the highest levels of necrotic and apoptotic cells, validating the excellent therapeutic efficacy of the co-delivery system mediated by the developed 1-C12G1 micelles. This trend was also confirmed by quantification of the cell apoptosis rate based on the population of TUNEL-positive cells in the tumor sections (Fig. S18, ESI†). The tumor cell apoptosis rate is in an order of 1-C12G1@DOX/miR-21i (87.3 ± 3.4%) > 1-C12G1@DOX (78.3 ± 6.4%) > free DOX (54.2 ± 2.4%) > 1-C12G1/miR-21i (39.6 ± 1.4%) > 1-C12G1 (3.0 ± 0.3%) > NS (1.0 ± 0.2%). These results match the results

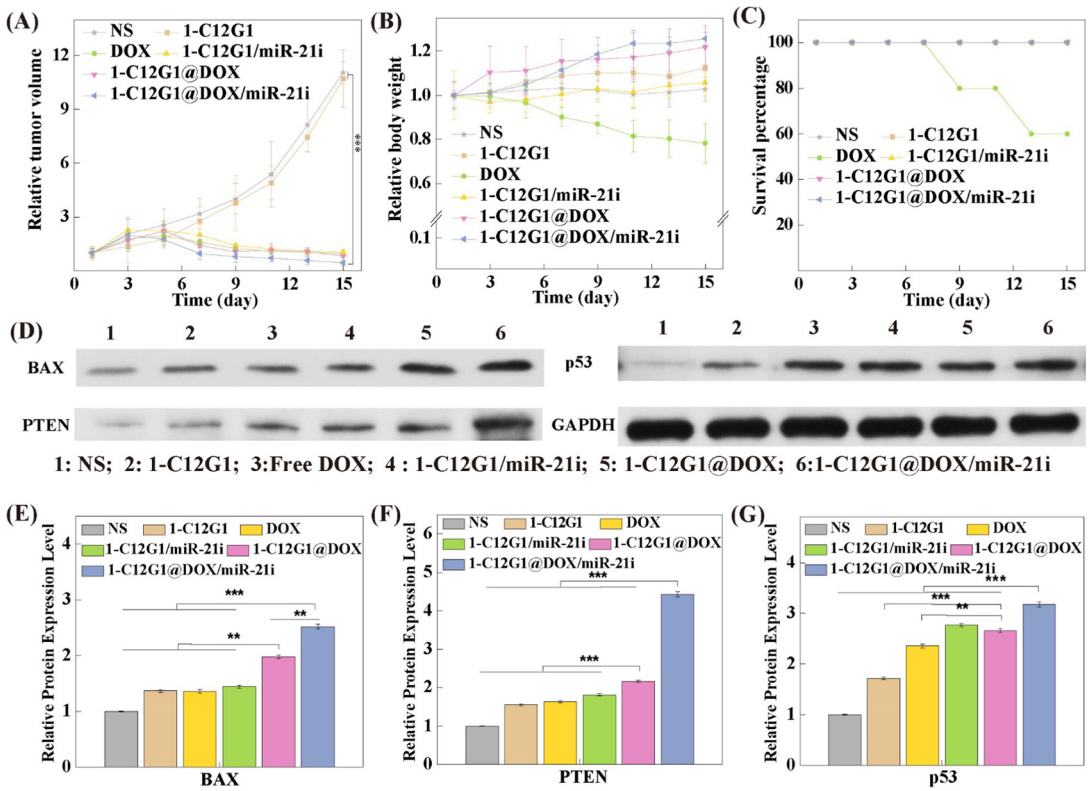

Fig. 6 (A) Relative tumor volume measured at given time points after different treatments ($n = 5$ for each group). (B) The relative body weights of mice in different treatment groups *versus* time post treatments ($n = 5$ for each group). (C) The survival rates of mice measured at given time points after different treatments. (D) Western blot assay of the expression of protein relevant to cell apoptosis in xenografted tumor cells in the treatment groups of 1-C12G1, free DOX, 1-C12G1/miR-21i, 1-C12G1@DOX or 1-C12G1@DOX/miR-21i (the equivalent DOX concentration was 1 μM). NS was used as control. (C–E) Quantification of the expression levels of cell apoptosis-related proteins of BAX (E), PTEN (F) and p53 (G) in the western blot data *in vivo* (* $p < 0.05$, ** $p < 0.01$, and *** $p < 0.005$, respectively).

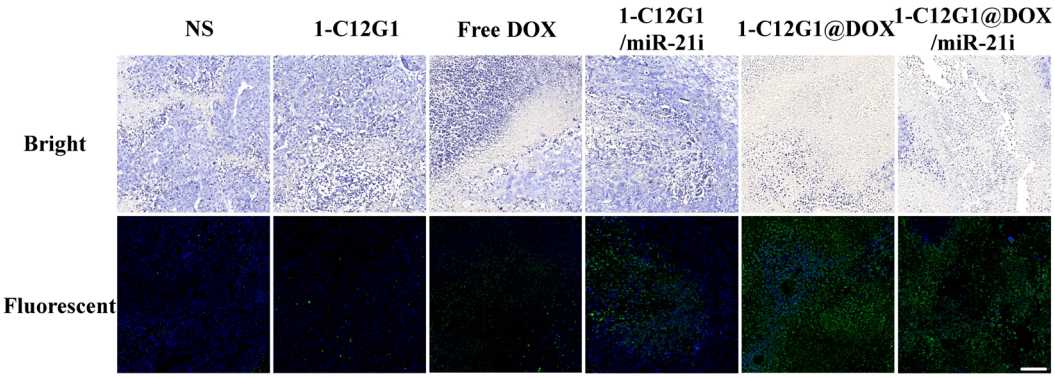

Fig. 7 TUNEL staining of the tumor sections from mice treated with NS, 1-C12G1, free DOX, 1-C12G1/miR-21i, 1-C12G1@DOX or 1-C12G1@DOX/miR-21i for 16 days. Scale bar in each panel represents 100 μm.

obtained above using flow cytometry (Fig. 3D). Apparently, the developed 1-C12G1 micelles with a nanoscale size are able to co-deliver both DOX and miR-21i to the tumor region through the passive enhanced permeability and retention (EPR) effect, theraby exerting a synergistic tumor chemo/gene therapeutic efficacy.

The histological features of the main organs of mice in different groups were also investigated through H&E staining (Fig. 8). Obviously, liver damage can be seen in the free DOX group. To be opposed, no visible organ damage is observed in the groups of 1-C12G1@DOX and 1-C12G1@DOX/miR-21i polyplexes (Fig. 8). The significantly alleviated toxicity of 1-C12G1@DOX and 1-C12G1@DOX/miR-21i polyplexes can be ascribed to the micellar formulation of DOX and miR-21i, which can be accumulated in the tumor site *via* the passive EPR-mediated targeting. Taken together, our results indicate that the developed 1-C12G1@DOX/miR-21i polyplexes can be used to co-deliver both DOX and miR-21i to exert improved tumor inhibition efficacy while reducing the systemic toxicity of DOX *via* rapid drug release at slightly acidic tumoral pH and the passive EPR effect.

Experimental

Preparation and characterization of amphiphilic phosphorus dendrons

As shown in Fig. 1, we prepared an amphiphilic phosphorus dendron bearing a long alkyl chain ($C_{12}H_{25}$) directly grafted on the N_3P_3 core and ten protonated pyrrolidine groups on the surface. This amphiphilic phosphorus dendron as well as all the intermediate products were synthesized in good overall yields. The AB_5 monomer (3) was synthesized through condensation of 4-hydroxybenzaldehyde (2) with hexachlorocyclotriphosphazene

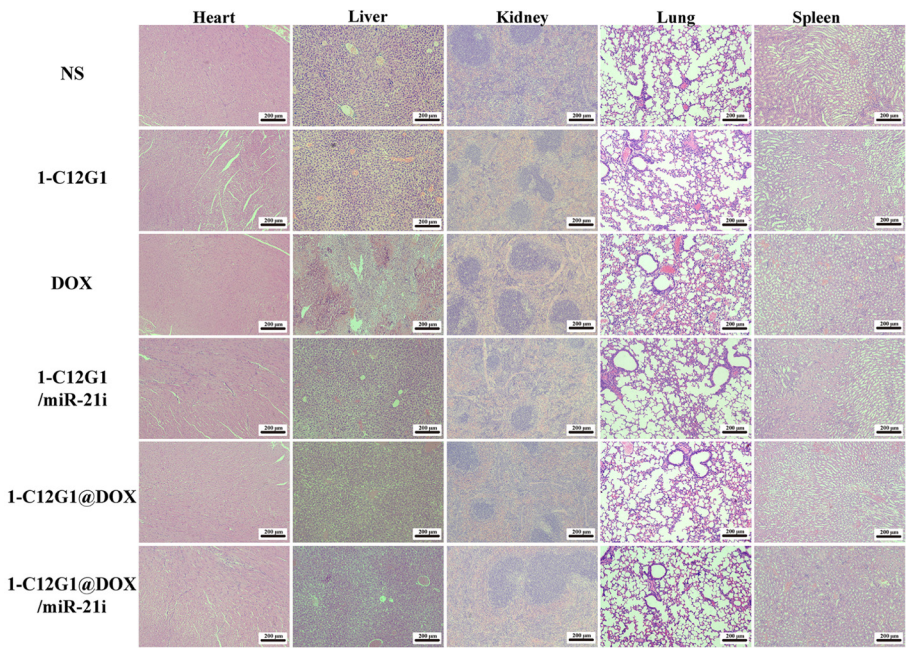

Fig. 8 H&E-stained organ sections from mice in the NS, 1-C12G1, free DOX, 1-C12G1/miR-21i, 1-C12G1@DOX or 1-C12G1@DOX/miR-21i treatment group for 16 days. Scale bar in each panel represents 200 μm.

(1) (THF, room temperature) to have a 76% yield. Next, by reacting 3 with the amino-phenol-derivative (4) (cesium carbonate, THF, room temperature), the dendron 5 was synthesized in an 80% yield. Further reaction of 5 with (1-methylhydrazinyl) phosphonothioic dichloride (6) (dichloromethane) at room temperature led to the synthesis of 7 (92% yield), which in turn was reacted with 1-(2-aminoethyl) pyrrolidine (8) (cesium carbonate, THF) at room temperature to produce the dendron C12G1NC4 in a 95% yield. Lastly, the pyrrolidine groups of C12G1NC4 were protonated in THF at room temperature to give the corresponding water-soluble amphiphilic dendrons 1-C12G1 in a 95% yield. Each product was characterized *via* different NMR techniques.

Preparation of 1-C12G1@DOX/miR-21i polyplexes

The 1-C12G1@DOX micelles were formed through incubation of 1-C12G1 and appropriate amount of hydrophobic DOX under different molar ratios (1-C12G1/DOX = 1 : 15, 1 : 20, 1 : 25, 1 : 30 and 1 : 35, respectively). Each mixture was stirred overnight at room temperature, and centrifuged (7000 rpm for 20 min) to remove the precipitates related to non-encapsulated DOX. The supernatant was then freeze-dried for up to 3 days to acquire the 1-C12G1@DOX complexes. Later, miR-21i and appropriate amount of 1-C12G1@DOX were mixed under various N/P values in diethyl procarbonate (DEPC) water and incubated for 30 min at room temperature to form the 1-C12G1@DOX/miR-21i polyplexes.

Cell culture and *in vitro* anti-proliferative activity

Human triple-negative breast cancer cells (MDA-MB-231 cells) and mouse normal fibroblast cells (NIH-3T3 cells) were regularly cultured in medium supplemented with 10% fetal bovine serum and 1% penicillin-streptomycin. Cells were treated with the 1-C12G1@DOX/miR-21i polyplexes for a certain period of time to examine their cytotoxicity, cellular uptake, and anticancer mechanisms.

Animal experiments

All animal experiments were approved by the ethical committee for animal care of Donghua University and also following the regulations of the National Ministry of Health (China). The tumor-bearing mice were intravenously injected with 0.9% normal saline (NS, Group 1), 1-C12G1 (Group 2), free DOX (Group 3), 1-C12G1/miR-21i (Group 4), 1-C12G1@DOX (Group 5), and 1-C12G1@DOX/miR-21i (Group 6) every 3 days for 5 times, respectively. Each mouse was injected with the dose of 5 mg DOX kg^{-1} or 1.2 mg 1-C12G1 kg^{-1}. We examined the tumor volumes and the body weights every two days. At 16 days post treatment, the mice were sacrificed to extract the tumor tissues and the main organs (heart, liver, spleen, lung, and kidney) for hematoxylin-eosin (H&E) and TdT-mediated dUTP Nick-End Labeling (TUNEL) staining according to standard protocols. For more details, please see the ESI.†

Conclusions

We developed amphiphilic phosphorus dendron (1-C12G1) micelles as a platform to co-deliver anticancer drug DOX and miR-21i, a genetic tumor suppressive material for synergistic therapy of TNBC. The unique structural features of the dendron micelles having a mean size of 25 nm include hydrophobic interior space and the positive surface potential, making them suitable to effectively load DOX and compress miR-21i. The created 1-C12G1@DOX/miR-21i polyplexes display a pH-sensitive DOX release profile, and can be efficiently taken up by cancer cells to exert their functions from both DOX and miR-21i to efficiently inhibit the growth of cancer cells *in vitro* and an orthotopic TNBC model *in vivo*. Furthermore, the developed dendron micelle-mediated delivery is beneficial to alleviate the free DOX-induced organ damage, thereby significantly improving the bioavailability of the drug. This newly developed phosphorous dendron-based micellar delivery system may be developed to co-deliver different drug/gene combinations for different synergistic therapy applications.

Author contributions

Liang Chen: methodology, data curation, software, writing – original draft. Mengsi Zhan: methodology, software, data curation. Jin Li: methodology, data curation. Liu Cao: methodology, data curation. Huxiao Sun: methodology, data curation. Régis Laurent: methodology, data curation. Serge Mignani: methodology, supervision, resources. Anne-Marie Caminade: supervision, resources, writing – review & editing. Jean-Pierre Majoral: supervision, resources, writing – review & editing. Xiangyang Shi: supervision, resources, funding acquisition, conceptualization, project administration, writing – review & editing.

Conflicts of interest

There are no conflicts to declare.

Acknowledgements

This research has been financially supported by the National Natural Science Foundation of China (81761148028 and 22150410324), the Science and Technology Commission of Shanghai Municipality (21490711500), Shanghai Municipal Health Commission (20214Y0133), China Postdoctoral Science Foundation (2022M712130), and the Shanghai Education Commission through the Shanghai Leading Talents Program. J. P. M., S. M., A. M. C. and R. L. thank the collaborative NSFC-CNRS grant (from the France part) for financial support. X. S. also thanks the support by FCT-Fundação para a Ciência e a Tecnologia through the CQM Base Fund - UIDB/00674/2020, and Programmatic Fund - UIDP/00674/2020, and by ARDITI-Agência Regional para o Desenvolvimento da Investigação Tecnologia e Inovação, through the project M1420-01-0145-FEDER-000005 - Centro de Química da Madeira - CQM^{+} (Madeira 14-20 Program).

Notes and references

1 R. J. Youle and A. Strasser, *Nat. Rev. Mol. Cell Biol.*, 2008, **9**, 47–59.
2 L. Zhang, Z. Lu, Q. Zhao, J. Huang, H. Shen and Z. Zhang, *Small*, 2011, **7**, 460–464.
3 X. Deng, M. Cao, J. Zhang, K. Hu, Z. Yin, Z. Zhou, X. Xiao, Y. Yang, W. Sheng, Y. Wu and Y. Zeng, *Biomaterials*, 2014, **35**, 4333–4344.
4 D. P. Bartel, *Cell*, 2004, **116**, 281–297.
5 E. Huntzinger and E. Izaurralde, *Nat. Rev. Genet.*, 2011, **12**, 99–110.
6 D. Hanahan and R. A. Weinberg, *Cell*, 2011, **144**, 646–674.
7 A. W. Tong and J. Nemunaitis, *Cancer Gene Ther.*, 2008, **15**, 341–355.
8 L. Lin, Y. Fan, F. Gao, L. Jin, D. Li, W. Sun, F. Li, P. Qin, Q. Shi, X. Shi and L. Du, *Theranostics*, 2018, **8**, 1923–1939.
9 T. J. Lee, J. Y. Yoo, D. Shu, H. Li, J. Zhang, J.-G. Yu, A. C. Jaime-Ramirez, M. Acunzo, G. Romano, R. Cui, H.-L. Sun, Z. Luo, M. Old, B. Kaur, P. Guo and C. M. Croce, *Mol. Ther.*, 2017, **25**, 1544–1555.
10 M. L. Si, S. Zhu, H. Wu, Z. Lu, F. Wu and Y. Y. Mo, *Oncogene*, 2007, **26**, 2799–2803.
11 C. Song, Y. Xiao, Z. Ouyang, M. Shen and X. Shi, *J. Mater. Chem. B*, 2020, **8**, 2768–2774.
12 D. Cheng, N. Cao, J. Chen, X. Yu and X. Shuai, *Biomaterials*, 2012, **33**, 1170–1179.
13 H. Wang, Y. Zhao, Y. Wu, Y.-L. Hu, K. Nan, G. Nie and H. Chen, *Biomaterials*, 2011, **32**, 8281–8290.
14 C.-M. J. Hu, S. Aryal and L. Zhang, *Ther. Delivery*, 2010, **1**, 323–334.
15 M. Creixell and N. A. Peppas, *Nano Today*, 2012, **7**, 367–379.
16 T. Wei, C. Chen, J. Liu, C. Liu, P. Posocco, X. Liu, Q. Cheng, S. Huo, Z. Liang, M. Fermeglia, S. Pricl, X.-J. Liang, P. Rocchi and L. Peng, *Proc. Natl. Acad. Sci. U. S. A.*, 2015, **112**, 2978–2983.
17 H. Cabral, Y. Matsumoto, K. Mizuno, Q. Chen, M. Murakami, M. Kimura, Y. Terada, M. R. Kano, K. Miyazono, M. Uesaka, N. Nishiyama and K. Kataoka, *Nat. Nanotechnol.*, 2011, **6**, 815–823.
18 V. P. Chauhan, T. Stylianopoulos, J. D. Martin, Z. Popovic, O. Chen, W. S. Kamoun, M. G. Bawendi, D. Fukumura and R. K. Jain, *Nat. Nanotechnol.*, 2012, **7**, 383–388.
19 T. Xiao, W. Hou, X. Cao, S. Wen, M. Shen and X. Shi, *Biomater. Sci.*, 2013, **1**, 1172–1180.
20 Y. Luo, Y. Li, Z. Huang, X. Li, Y. Wang, J. Hou and S. Zhou, *Nano Lett.*, 2022, **22**, 6418–6427.
21 Y. Wang, G. Wei, X. Zhang, X. Huang, J. Zhao, X. Guo and S. Zhou, *Small*, 2018, **14**, 1702994.
22 F. Abedi-Gaballu, G. Dehghan, M. Ghaffari, R. Yekta, S. Abbaspour-Ravasjani, B. Baradaran, J. E. N. Dolatabadi and M. R. Hamblin, *Appl. Mater. Today*, 2018, **12**, 177–190.
23 X. X. Liu, J. H. Zhou, T. Z. Yu, C. Chen, Q. Cheng, K. Sengupta, Y. Y. Huang, H. T. Li, C. Liu, Y. Wang, P. Posocco, M. H. Wang, Q. Cui, S. Giorgio, M. Fermeglia, F. Q. Qu, S. Pricl, Y. H. Shi, Z. C. Liang, P. Rocchi, J. J. Rossi and L. Peng, *Angew. Chem., Int. Ed.*, 2014, **53**, 11822–11827.
24 D. Wang, Y. L. Chen, Y. Gao, C. Song, Z. Ouyang, J. C. Li, S. S. Mignani, J. Majoral, X. Shi and Y. M. W. Shen, *J. Mater. Chem. B*, 2021, **9**, 6149–6154.
25 J. Li, L. Chen, C. Li, Y. Fan, M. Zhan, H. Sun, S. Mignani, J.-P. Majoral, M. Shen and X. Shi, *Theranostics*, 2022, **12**, 3407–3419.
26 L. Chen, L. Cao, M. S. Zhan, J. Li, D. Y. Wang, R. Laurent, S. Mignani, A. M. Caminade, J. P. Majoral and X. Y. Shi, *Biomacromolecules*, 2022, **23**, 2827–2837.
27 V. Percec, D. A. Wilson, P. Leowanawat, C. J. Wilson, A. D. Hughes, M. S. Kaucher, D. A. Hammer, D. H. Levine, A. J. Kim, F. S. Bates, K. P. Davis, T. P. Lodge, M. L. Klein, R. H. DeVane, E. Aqad, B. M. Rosen, A. O. Argintaru, M. J. Sienkowska, K. Rissanen, S. Nummelin and J. Ropponen, *Science*, 2010, **328**, 1009–1014.
28 T. Xiao, X. Cao, W. Hou, C. Peng, J. Qiu and X. Shi, *J. Nanosci. Nanotechnol.*, 2015, **15**, 10134–10140.
29 S. D. Conner and S. L. Schmid, *Nature*, 2003, **422**, 37–44.
30 S. Mura, J. Nicolas and P. Couvreur, *Nat. Mater.*, 2013, **12**, 991–1003.
31 V. P. Torchilin, *Nat. Rev. Drug Discovery*, 2014, **13**, 813–827.
32 G. Li, Y. Fan, L. Lin, R. Wu, M. Shen and X. Shi, *Sci. China: Chem.*, 2021, **64**, 817–826.
33 L. Li, L. Yuan, J. Luo, J. Gao, J. Guo and X. Xie, *Clin. Exp. Med.*, 2013, **13**, 109–117.
34 S.-J. Kim, J.-S. Oh, J.-Y. Shin, K.-D. Lee, K. W. Sung, S. J. Nam and K.-H. Chun, *J. Controlled Release*, 2011, **155**, 427–434.
35 S. Raj, V. I. Franco and S. E. Lipshultz, *Curr. Treat. Options Cardiovasc. Med.*, 2014, **16**, 315.
36 Y. Octavia, C. G. Tocchetti, K. L. Gabrielson, S. Janssens, H. J. Crijns and A. L. Moens, *J. Mol. Cell. Cardiol.*, 2012, **52**, 1213–1225.
37 E. H. Herman, A. N. Elhage, V. J. Ferrans and B. Ardalan, *Toxicol. Appl. Pharmacol.*, 1985, **78**, 202–214.